

# Probing the Faintest Stars in a Globular Star Cluster

Harvey B. Richer,<sup>1\*</sup> Jay Anderson,<sup>2</sup> James Brewer,<sup>1</sup> Saul Davis,<sup>1</sup> Gregory G. Fahlman,<sup>3</sup> Brad M. S. Hansen,<sup>4</sup> Jarrod Hurley,<sup>5</sup> Jasonjot S. Kalirai,<sup>6</sup> Ivan R. King,<sup>7</sup> David Reitzel,<sup>4</sup> R. Michael Rich,<sup>4</sup> Michael M. Shara,<sup>8</sup> Peter B. Stetson<sup>3</sup>

NGC 6397 is the second closest globular star cluster to the Sun. Using 5 days of time on the Hubble Space Telescope, we have constructed an ultradeep color-magnitude diagram for this cluster. We see a clear truncation in each of its two major stellar sequences. Faint red main-sequence stars run out well above our observational limit and near to the theoretical prediction for the lowest mass stars capable of stable hydrogen burning in their cores. We also see a truncation in the number counts of faint blue stars, namely white dwarfs. This reflects the limit to which the bulk of the white dwarfs can cool over the lifetime of the cluster. There is also a turn toward bluer colors in the least luminous of these objects. This was predicted for the very coolest white dwarfs with hydrogen-rich atmospheres as the formation of H<sub>2</sub> and the resultant collision-induced absorption cause their atmospheres to become largely opaque to infrared radiation.

When stars are born, they contract under gravity, increasing their central temperatures and densities. If a star is massive enough, at least 0.08 that of the Sun (80 times the mass of Jupiter), the center will eventually get hot enough to allow self-sustaining nuclear energy generation at a level sufficient to halt the contraction. For lower mass objects, the contraction is halted instead by electron degeneracy, the quantum mechanical repulsion between electrons in dense media. For these “brown dwarfs,” the rate of energy generation never grows large enough to be self-sustaining, and they fade away within a billion years (1). On the other hand, for low-mass stars just above the brown dwarf mass limit, the balance between gravity and thermal equilibrium is long-lived, and these stars are able to shine for much longer than the current age (13.7 billion years) of the universe (2). The sharp division between transient and effectively infinite lifetime populations is termed the hydrogen-burning mass limit and is a cornerstone of stellar evolutionary theory. However, because of the faintness of the stars just above the limit, this edge has not previously

been solidly identified in any old stellar population such as globular clusters or halo field stars.

At the other end of the stellar mass spectrum, stars with masses ranging from about 1 through 7 solar masses consume their nuclear fuel on a time scale shorter than the age of the universe, burning their original hydrogen to carbon and oxygen, ejecting their outer layers, and becoming white dwarfs. These stellar remnants are also supported by electron degeneracy pressure and slowly cool over time as they radiate their reservoir of thermal energy left over from the previous stages of nuclear burning. The accompanying slow fading, at approximately constant radius, traces out the so-called white dwarf cooling sequence in the color-magnitude diagram (CMD). At faint magnitudes, this sequence is expected to end, with the magnitude of the cutoff indicating the luminosity to which the oldest white dwarfs have faded. With the aid of theoretical models, this luminosity can then be used to derive the age of the cluster (3, 4).

The white dwarf cooling sequence is expected to turn back to the blue at faint magnitudes (5–9). As white dwarfs with hydrogen-rich atmospheres cool below temperatures of 4000 K, they exhibit the collision-induced absorption (CIA) of molecular hydrogen (10). CIA is strongest at near-infrared wavelengths, which suppresses the flux near 1 μm (11) and causes the optical colors to become bluer as the star cools, rather than redder, as might be expected from a blackbody. CIA arises because hydrogen molecules can form in these cool atmospheres. Being symmetric, H<sub>2</sub> does not have a dipole moment and will only very weakly absorb radiation via quadrupole transitions (10). A dipole moment may be induced, however, during an H<sub>2</sub>-H<sub>2</sub>, H<sub>2</sub>-H, or H<sub>2</sub>-He collision (12), leading to CIA. The stars continue to get bolometrically fainter and cooler as they evolve

on the blueward track in the CMD known as the blue hook. The spectral signature of CIA has been seen in a few individual field white dwarfs (13–15), but never as a feature in the cooling sequence of a stellar cluster. The expected cluster CIA signature is a blue hook in the cooling sequence. We note that this is a temperature effect, seen at faint magnitudes, and that it is distinct from the feature observed in the open cluster NGC 6791 (16). The latter feature occurs in younger populations and is a consequence of the smaller radii and slower cooling of more massive white dwarfs at early times, as shown in figure 17 of (17).

**Imaging data.** In an attempt to locate the limits of both the faint main-sequence star population and the faint white dwarf population, we used the Hubble Space Telescope (HST) to obtain images of the globular star cluster NGC 6397 located in the southern constellation Ara. It is seen projected in the direction of the galactic center, at a distance of about 8500 light-years from Earth (18), and its stars have a heavy-element content that is ~1% that of the Sun (19). It was discovered by Abbé Nicolas Louis de Lacaille during his sojourn at the Cape of Good Hope in 1751–1752; in his original catalog, it bears the name Lacaille III.11. It was the 12th such cluster discovered. We imaged a single field in NGC 6397 with the Advanced Camera for Surveys (ACS) on the HST for a total of 126 orbits (4.7 days) to characterize the faintest globular cluster stellar populations. Our observations were carried out 5 arc min southeast of the cluster core. They overlap preexisting Wide Field Planetary Camera 2 (WFPC2) images that we used to select, by common proper motion (angular motion in the plane of the sky), a clean sample of cluster stars largely devoid of galactic foreground and background stars. The exposures were taken through two filters, F606W and F814W, where the number indicates the central wavelength of the filter in nanometers.

The data set consists of 252 exposures totaling 179.7 ksec in F814W and 126 exposures totaling 93.4 ksec in F606W. This 2:1 ratio was chosen because the primary science goal of the program was exploration for the coolest white dwarfs. If cool white dwarfs do indeed turn blue at faint magnitudes (5–9), they will be very faint on the longer wavelength images, thus requiring increased exposure time to detect them. To find the faintest possible sources, we scoured each image for indications of where the faintest stars might be located. The most we could hope for from the very faintest ones is that they would push their central pixels up above the noise in some significant number of images. We studied the noise in the images via artificial star tests, and we concluded that a detection in 90 out of 252 F814W images constituted a 3σ detection above the background.

Figure 1 is an image of part of our field that was constructed by combining the exposures in

<sup>1</sup>Department of Physics and Astronomy, University of British Columbia, Vancouver, British Columbia V6T 1Z1, Canada. <sup>2</sup>Department of Physics and Astronomy, Rice University, Houston, TX 77005, USA. <sup>3</sup>National Research Council, Herzberg Institute of Astrophysics, Victoria, British Columbia V9E 2E7, Canada. <sup>4</sup>Division of Astronomy and Astrophysics, University of California, Los Angeles, CA 90095, USA. <sup>5</sup>Department of Mathematics and Statistics, Monash University, Clayton, Victoria 3800, Australia. <sup>6</sup>Department of Astronomy and Astrophysics, University of California, Santa Cruz, CA 95064, USA. <sup>7</sup>Department of Astronomy, University of Washington, Seattle, WA 98195, USA. <sup>8</sup>Department of Astrophysics, American Museum of Natural History, New York, NY 10024, USA.

\*To whom correspondence should be addressed. E-mail: richer@astro.ubc.ca

the two filters. The insets provide expanded views of two stars at the extremities of stellar evolution: the least luminous hydrogen-burning cluster star observed (bottom) and a white dwarf that is cool enough to lie in the blue hook part of the cooling sequence (top).

**Cluster CMD.** We constructed a CMD (Fig. 2A) from these data, including all sources that (i) generated local maxima in at least 90 out of 252 F814W images, (ii) were the most significant sources within 7.5 ACS pixels, and (iii) passed morphology tests indicating that they are point-like objects. In this diagram, brighter stars have small values of the F814W magnitude and

red stars will have larger positive ( $F606W - F814W$ ) colors. Some unresolved faint blue galaxies likely remain in the sample bluer than ( $F606W - F814W$ ) = 1 and fainter than  $F814W = 27$ . To estimate the photometric errors for white dwarf stars, we used measurements of artificial stars of known magnitude inserted into the individual exposures and recovered by our finding and measuring algorithms. In addition, we considered the completeness for stars as a function of the F814W magnitude—that is, the fraction of stars that we recovered in the ACS images in artificial star tests. The completeness is based solely on the recovery fractions in the F814W

data and hence applies equally well to both white dwarfs and main-sequence stars. Completeness fractions in excess of 50% are normally considered acceptable.

Figure 2A is dominated by a narrow continuous cluster sequence spanning at least 14 magnitudes in the F814W filter. The sequence extends from a sparse giant branch at the brightest F814W magnitudes, through the main-sequence turnoff near  $F814W = 15.7$ , and down the main sequence to faint objects, with a possible termination in a cloud of field stars near  $F814W = 24$ . The turnoff region corresponds to stars that have recently completed hydrogen burning in their cores. They will shortly evolve into red giants, a phase of evolution lasting about 100 million years, before they eject their atmospheres and become white dwarfs. The scatter around this narrow sequence is produced by stars not associated with the cluster. These are stars from the galactic disk and bulge that are found along the line of sight to NGC 6397. This population is large because of the low galactic latitude ( $-12^\circ$ ) of NGC 6397.

The most novel feature of the diagram, however, is the white dwarf cooling sequence, which begins at about  $F814W = 22.5$  and extends to  $F814W = 27.2$ , where it then “hooks” toward the blue. The sequence appears to be largely truncated fainter than  $F814W = 27.8$ . This truncation reflects the limit to which the bulk of the hydrogen-rich white dwarfs can cool over the lifetime of the cluster. For this reason it will be a powerful diagnostic in determining the age of NGC 6397. However, this truncation does not necessarily mean that there are no white dwarfs in the cluster fainter than this limit. Over a long period of time, both massive white dwarfs (those with masses in excess of about 0.8 that of the Sun) and those with helium-rich atmospheres cool more quickly and to fainter magnitudes than do white dwarfs of modest mass (0.5 to 0.6 solar masses) with hydrogen-rich atmospheres. As a consequence of electron degeneracy, more massive white dwarfs have smaller radii and hence larger densities. They will thus develop a crystallized core earlier than low-mass white dwarfs, causing them to enter a regime known as Debye cooling before the lower mass ones do. In this phase of evolution, the star effectively loses its ability to store thermal energy and it cools very rapidly. Because helium does not form molecules (which would have a vibrational mode), white dwarfs with pure helium atmospheres do not suffer from CIA. Their atmospheres are thus less opaque to infrared radiation and they cool rapidly. Hence, both massive and helium-rich white dwarfs may have cooled to below our observational limit.

We examined the details of the CMD further by analyzing the stars whose proper motions match that of the cluster (Fig. 2B and Fig. 3). Preexisting WFPC2 images, which were

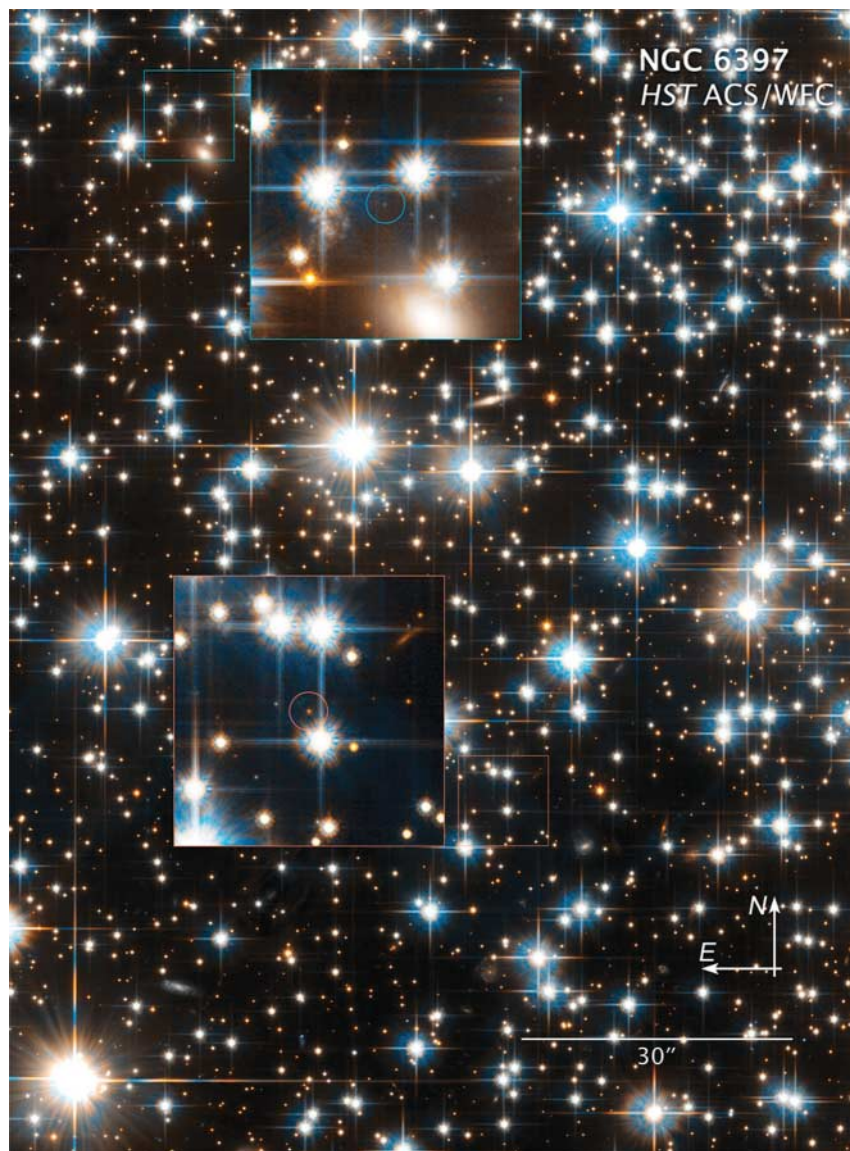


**Fig. 1.** A section of the observed field in NGC 6397 covering 94 arc sec by 127 arc sec. This is 29% of the entire field of our observations. Directions on the sky and a scale bar are shown at the lower right. The image is a composite of exposures from the HST ACS wide-field camera in F606W and F814W. The insets (each 10 arc sec by 10 arc sec) show detail for the faintest hydrogen-burning star observed in the cluster (top) and a white dwarf along the blue hook part of the cooling sequence (bottom). Although the field is in a globular star cluster with many bright stars, the ACS has such a tight point spread function, with relatively little scattered light, that it is still possible to see faint external galaxies right through the cluster.

used to proper motion-clean the data, overlap only 60% of the area of the ACS field and are much shorter in exposure time (F814W exposure times of 3960, 7440, and 5200 s in each of the 1994, 1997 and 2001 data sets, versus 179.7 ksec with the ACS in 2005) so that their utility, particularly for the very faintest stars, was limited. Distinguishing between cluster and field stars is a serious issue for stars along the main sequence as well as those in the white dwarf region. The main-sequence stars become very red at faint magnitudes, so they may be found on the F814W images but could be unmeasurable on the bluer F606W frames. For the white dwarfs, if they do indeed become bluer as they cool (5–9), we might expect to lose them on the F814W frames. Nonetheless, the major features are preserved and are much cleaner in Fig. 2B than in Fig. 2A. The main sequence is now seen

to continue to  $F814W \sim 26.0$  at  $(F606W - F814W) \sim 4.0$ . An F814W magnitude of 26.0 and a F606W magnitude of 30.0 correspond to absolute magnitudes of 13.6 and 17.4, respectively. These absolute magnitudes are more than a full magnitude fainter than the faintest known metal-poor (“population II”) field stars (20, 21), which suggests that there remains a population of extremely dim metal-poor stars awaiting discovery in the halo of the galaxy.

The cluster main sequence has two remarkable features: one at  $F814W \sim 24$ , where the number counts of stars decline rapidly [noted by (22)], and another at  $F814W \sim 26$ , where the main sequence appears to terminate. This latter feature is not caused by incompleteness (Fig. 3). Except for a few stars that scatter well away from the main-sequence locus (all these are also outliers in the proper motion distribu-

tion, so they are likely interlopers from the field population), there appears to be a complete lack of cluster main-sequence stars fainter than  $F814W = 26$ . The presence of an extensive white dwarf population as faint as  $F814W = 27.8$ , as well as numerous faint field stars, shows that if a significant population of main-sequence stars fainter than  $F814W = 26$  were present, we would have found it.

**Proper motions.** We quantified this result by examining the proper motion distribution for faint red and blue stars (Fig. 3). NGC 6397 is moving relative to the field stars. Over the course of 10 years since the first archival data were taken, the cluster stars have moved by almost 3 ACS pixels with respect to the bulk of those in the field. A displacement this large is trivial to measure, provided we can find the star in the archival data. Figure 3 displays the proper motions for all objects with respect to the cluster as a function of F814W magnitude. The proper motion cuts we made to select cluster stars are shown in Fig. 3A; these stars are all to the left of the red line, which is set by fitting a Gaussian function to the total proper motion distribution in bins one magnitude wide and selecting those stars that lie within two standard deviations from the mean. The remaining plots are proper motions along the detector axes for stars redder than  $(F606W - F814W) = 1.5$  (Fig. 3, B to D) and for blue stars with  $(F606W - F814W) < 1.5$  (Fig. 3E). The circle shown in each plot is the proper motion cut appropriate to that magnitude. The circle has a radius of 0.5 ACS pixels in Fig. 3B and 1.3 pixels in Fig. 3, D and E. By contrast, proper motion errors in  $x$  and  $y$  range from 0.05 pixels at  $F814W = 22$  to 0.6 pixels at  $F814W = 26$ . It is clear that clumps corresponding to cluster stars are seen in Fig. 3, B and C, but that no concentration is seen for red main-sequence stars with  $F814W > 26$  (Fig. 3D). This coincides with the impression in Fig. 2B that there are no obvious cluster stars fainter than this limit. Figure 3E illustrates the displacements for stars with  $(F606W - F814W) < 1.5$  and  $F814W > 26$ , which includes cluster white dwarfs, blue field stars, and unresolved blue galaxies. Clearly, there is a sizable component of stars moving with the cluster at these faint magnitudes (the white dwarfs), so that the deficiency seen for the main-sequence stars is real and not due to incompleteness.

**Hydrogen-burning limit.** The apparent termination of our observed main sequence lies close to the predicted hydrogen-burning limit (Fig. 2B, solid square); the lowest mass star capable of stable nuclear fusion of hydrogen in its core is 0.083 solar masses at the low heavy element abundance of NGC 6397 (23, 24). We caution, however, that different models may yield different results. At masses just above the hydrogen-burning limit, the relation between the mass and luminosity of a star is very steep; an extremely small change in mass results in a large

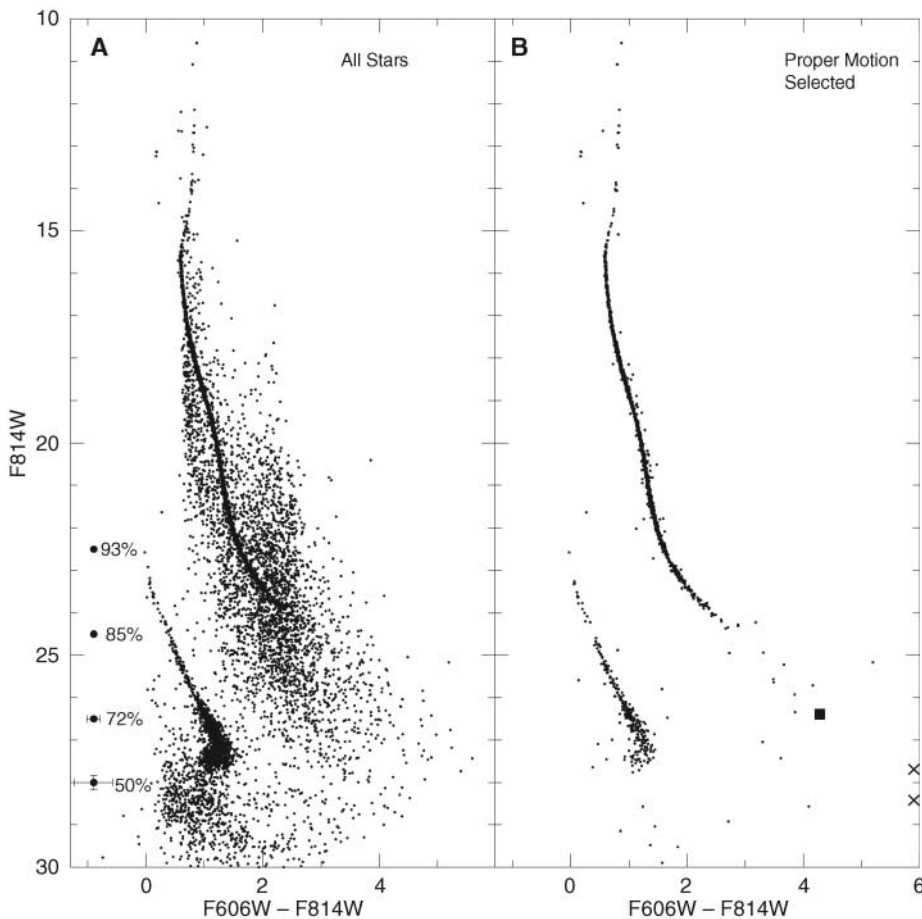


**Fig. 2.** The CMD of NGC 6397 (A) without proper motion selection of cluster members, and (B) after cleaning the data with the use of proper motions to exclude noncluster stars in the galactic disk and bulge from the sample (see also Fig. 3). Most of the faint galaxies and artifacts have been removed from (A) by requiring that the found objects pass certain morphological tests. The  $1\sigma$  photometric errors as a function of magnitude are indicated for white dwarfs by the error bars at  $F814W = 22.5, 24.5, 26.5$ , and  $28.0$ , as well as the percentage of stars (either white dwarfs or main sequence) found in the ACS images at each of these magnitudes from artificial star tests. In (B) the cluster main sequence appears to terminate at  $F814W = 26$ ,  $(F606W - F814W) = 4$ . The few scattered objects at lower luminosity are at the extremes of the proper motion selection criteria and are likely interlopers from the large field population. The two X's to the right indicate the F814W magnitudes of the stars that passed the proper motion cuts but whose F606W magnitudes were not measured. The solid square is the location of the hydrogen-burning limit for one particular set of theoretical models (23, 24).

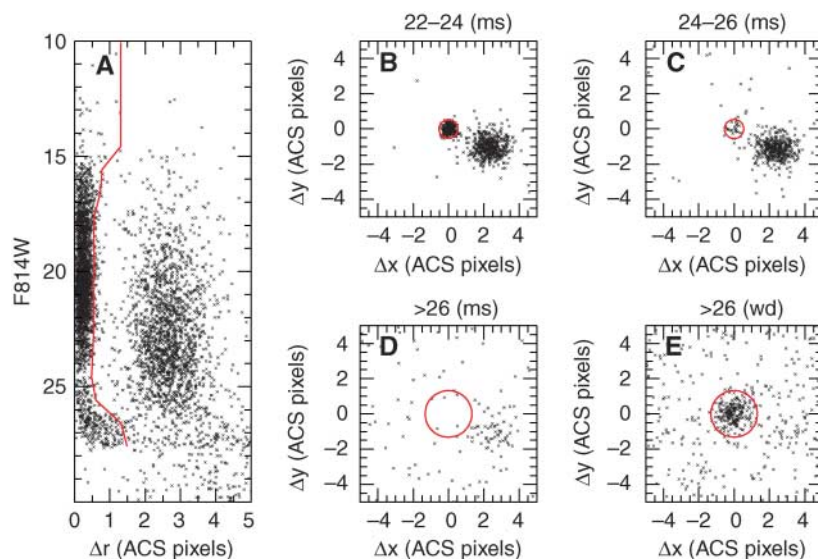


**Fig. 3.** (A) The F814W magnitude plotted against total stellar proper motion displacement  $\Delta r$  (scaled to 10 years) with respect to the cluster. The units are ACS pixels that project to 0.05 arc sec on the sky. The red line shows the selection criterion; all stars to the left of the line are considered to be cluster members. (B to E) Displacements in the  $x$  and  $y$  directions on the detector ( $-x$  is approximately north; ms, main sequence; wd, white dwarf). The NGC 6397 stars are those in the tight clump at (0,0); the bulk of the field stars are located in the diffuse clump about 3 pixels away.

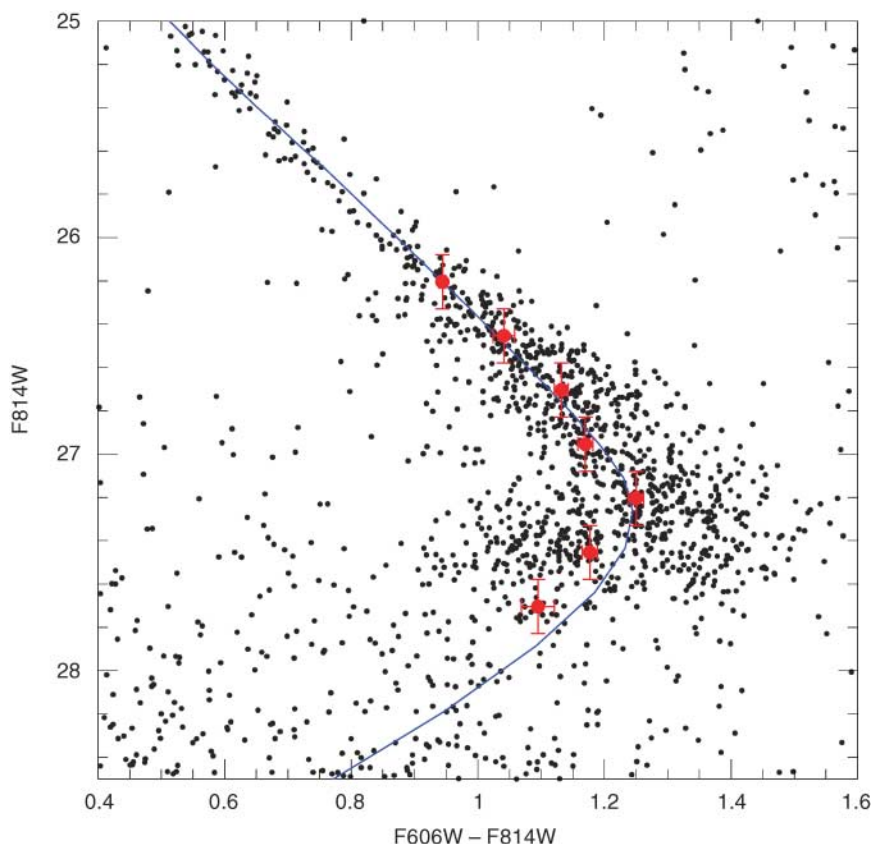


**Fig. 4.** The white dwarf region of the full CMD (i.e., not proper motion-cleaned) overlaid with the empirical cooling sequence (red dots with  $1\sigma$  error bars) derived as described in the text. We use the full CMD here in lieu of the proper motion-cleaned one to avoid artificial truncation of the cooling sequence from losses of stars from the shorter exposure, earlier epoch data. The solid blue curve is a theoretical cooling sequence using the atmospheric models of Bergeron *et al.* (7) and a cooling model for 0.5 solar mass white dwarfs of Hansen (6).

change in luminosity. This is because at low masses, electron degeneracy pressure becomes important in supporting the star. The temperature no longer increases with increasing pressure as it does for a classical gas. This has the effect of decreasing the central temperature and hence the nuclear energy generation rate (25). As stars approach the hydrogen-burning limit in mass, we thus expect to see a steep decline in their number counts as a function of luminosity. This makes it highly improbable that any stars will be found at the hydrogen-burning limit.

**Blue hook.** The blue hook feature in the white dwarf cooling sequence remains after proper motion cleaning, leading us to conclude that we are indeed seeing the predicted CIA signature (5–9). We quantified the nature of the hook by deriving an empirical cooling sequence. We fit the observed color distribution in F814W magnitude bins of width 0.25 with a model of the dispersion in color determined from artificial star tests. This resulted in a relation between color and magnitude that is purely empirical and can be compared to any theoretical models of the cooling. In Fig. 4, we show the comparison between this relation and one particular theoretical cooling sequence. Note that there is indeed a blue hook in the empirical relation and that we see excellent agreement between this and the model curve. This concordance suggests that further detailed modeling of these cool white dwarfs will provide a strong constraint on the white dwarf cooling age of NGC 6397.

**Final remarks.** In 1984, the late Vittorio Castellani and Vittoria Caloi suggested to the European Space Agency that HST be used to locate the end of the hydrogen-burning main sequence in the nearest globular star clusters. We believe that we have met this challenge. In addition, the blue hook and a truncation in the white dwarf cooling region have also been located. These features can now be exploited to learn more about the structure of low-mass stars, brown dwarfs, the original massive stellar component in globular clusters, white dwarf atmospheres and cooling, and ultimately the ages of these oldest known stellar populations.

#### References and Notes

1. A. Burrows, W. B. Hubbard, D. Saumon, J. I. Lunine, *Astrophys. J.* **406**, 158 (1993).
2. D. N. Spergel *et al.*, *Astrophys. J. Suppl. Ser.* **148**, 175 (2003).
3. G. Fontaine, P. Brassard, P. Bergeron, *Publ. Astron. Soc. Pac.* **113**, 409 (2001).
4. B. M. S. Hansen *et al.*, *Astrophys. J. Suppl. Ser.* **155**, 551 (2004).
5. B. M. S. Hansen, *Nature* **394**, 860 (1998).
6. B. M. S. Hansen, *Astrophys. J.* **520**, 680 (1999).
7. P. Bergeron, F. Wesemael, A. Beauchamp, *Publ. Astron. Soc. Pac.* **107**, 1047 (1995).
8. G. Chabrier, *Astrophys. J.* **513**, 103 (1999).
9. D. Saumon, S. B. Jacobson, *Astrophys. J.* **511**, L107 (1999).
10. C. Zheng, A. Borysow, *Astrophys. J.* **441**, 960 (1995).
11. A. Borysow, U. G. Jorgensen, Y. Fu, *J. Quant. Spectr. Rad. Trans.* **68**, 235 (2001).

12. M. Gustafsson, L. Frommhold, *Astron. Astrophys.* **400**, 1161 (2003).
13. H. C. Harris *et al.*, *Astrophys. J.* **524**, 1000 (1999).
14. S. T. Hodgkin *et al.*, *Nature* **403**, 57 (2000).
15. B. R. Oppenheimer *et al.*, *Astrophys. J.* **550**, 448 (2001).
16. L. R. Bedin *et al.*, *Astrophys. J.* **624**, L45 (2005).
17. B. M. S. Hansen, *Phys. Rep.* **399**, 1 (2004).
18. I. N. Reid, J. E. Gizis, *Astron. J.* **116**, 2929 (1998).
19. R. G. Gratton *et al.*, *Astron. Astrophys.* **408**, 529 (2003).
20. S. K. Leggett, F. Allard, P. H. Hauschildt, *Astrophys. J.* **509**, 836 (1998).
21. S. Lepine, M. M. Shara, R. M. Rich, *Astrophys. J.* **602**, L125 (2004).
22. I. R. King, J. Anderson, A. M. Cool, G. Piotto, *Astrophys. J.* **492**, L37 (1998).
23. I. Baraffe, G. Chabrier, F. Allard, P. H. Hauschildt, *Astron. Astrophys.* **327**, 1054 (1997).
24. The models in (23) have been updated (available at <http://perso.ens-lyon.fr/isabelle.baraffe>).
25. G. Chabrier, I. Baraffe, *Annu. Rev. Astron. Astrophys.* **38**, 337 (2000).
26. Supported by NASA/HST grant GO-10424 (J.A., B.M.S.H., I.R.K., J.S.K., R.M.R., M.M.S.), a NASA Hubble Fellowship (J.S.K.), the U.S.-Canada Fulbright Fellowship Committee (H.B.R.), the Natural Sciences and Engineering Research Council of Canada (H.B.R.), and the University of British

Columbia. H.B.R. thanks I. Ozier for fruitful discussions on CIA, as well as UCLA for support during his extended visit during which most of this paper was written. This research is based on NASA/ESA Hubble Space Telescope observations obtained at the Space Telescope Science Institute, which is operated by the Association of Universities for Research in Astronomy Inc. under NASA contract NAS5-26555. These observations are associated with proposal GO-10424.

31 May 2006; accepted 18 July 2006  
10.1126/science.1130691

# Warming and Earlier Spring Increase Western U.S. Forest Wildfire Activity

A. L. Westerling,<sup>1,2\*</sup> H. G. Hidalgo,<sup>1</sup> D. R. Cayan,<sup>1,3</sup> T. W. Swetnam<sup>4</sup>

Western United States forest wildfire activity is widely thought to have increased in recent decades, yet neither the extent of recent changes nor the degree to which climate may be driving regional changes in wildfire has been systematically documented. Much of the public and scientific discussion of changes in western United States wildfire has focused instead on the effects of 19th- and 20th-century land-use history. We compiled a comprehensive database of large wildfires in western United States forests since 1970 and compared it with hydroclimatic and land-surface data. Here, we show that large wildfire activity increased suddenly and markedly in the mid-1980s, with higher large-wildfire frequency, longer wildfire durations, and longer wildfire seasons. The greatest increases occurred in mid-elevation, Northern Rockies forests, where land-use histories have relatively little effect on fire risks and are strongly associated with increased spring and summer temperatures and an earlier spring snowmelt.

Wildfires have consumed increasing areas of western U.S. forests in recent years, and fire-fighting expenditures by federal land-management agencies now regularly exceed US\$1 billion/year (1). Hundreds of homes are burned annually by wildfires, and damages to natural resources are sometimes extreme and irreversible. Media reports of recent, very large wildfires (>100,000 ha) burning in western forests have garnered widespread public attention, and a recurrent perception of crisis has galvanized legislative and administrative action (1–3).

Extensive discussions within the fire-management and scientific communities and the media seek to explain these phenomena, focusing on either land-use history or climate as primary causes. If increased wildfire risks are driven primarily by land-use history, then ecological restoration and fuels management are potential solutions. However, if increased risks are largely due to changes in climate during recent decades, then restoration and fuels treatments may be relatively ineffective in reversing current wildfire trends (4, 5). We investigated

34 years of western U.S. (hereafter, “western”) wildfire history together with hydroclimatic data to determine where the largest increases in wildfire have occurred and to evaluate how recent climatic trends may have been important causal factors.

**Competing explanations: Climate versus management.** Land-use explanations for increased western wildfire note that extensive livestock grazing and increasingly effective fire suppression began in the late 19th and early 20th centuries, reducing the frequency of large surface fires (6–8). Forest regrowth after extensive logging beginning in the late 19th century, combined with an absence of extensive fires, promoted forest structure changes and biomass accumulation, which now reduce the effectiveness of fire suppression and increase the size of wildfires and total area burned (3, 5, 9). The effects of land-use history on forest structure and biomass accumulation are, however, highly dependent upon the “natural fire regime” for any particular forest type. For example, the effects of fire exclusion are thought to be profound in forests that previously sustained frequent, low-intensity surface fires [such as Southwestern ponderosa pine and Sierra Nevada mixed conifer (2, 3, 10, 11)], but of little or no consequence in forests that previously sustained only very infrequent, high-severity crown fires (such as Northern Rockies lodgepole pine or spruce-fir (1, 5, 12]).

In contrast, climatic explanations posit that increasing variability in moisture conditions (wet/dry oscillations promoting biomass growth, then burning), and/or a trend of increasing drought frequency, and/or warming temperatures have led to increased wildfire activity (13, 14). Documentary records and proxy reconstructions (primarily from tree rings) of fire history and climate provide evidence that western forest wildfire risks are strongly positively associated with drought concurrent with the summer fire season and (particularly in ponderosa pine-dominant forests) positively associated to a lesser extent with moist conditions in antecedent years (13–18). Variability in western climate related to the Pacific Decadal Oscillation and intense El Niño/La Niña events in recent decades along with severe droughts in 2000 and 2002 may have promoted greater forest wildfire risks in areas such as the Southwest, where precipitation anomalies are significantly influenced by patterns in Pacific sea surface temperature (19–22). Although corresponding decadal-scale variations and trends in climate and wildfire have been identified in paleo studies, there is a paucity of evidence for such associations in the 20th century.

We describe land-use history versus climate as competing explanations, but they may be complementary in some ways. In some forest types, past land uses have probably increased the sensitivity of current forest wildfire regimes to climatic variability through effects on the quantity, arrangement, and continuity of fuels. Hence, an increased incidence of large, high-severity fires may be due to a combination of extreme droughts and overabundant fuels in some forests. Climate, however, may still be the primary driver of forest wildfire risks on interannual to decadal scales. On decadal scales, climatic means and variability shape the character of the vegetation [e.g., species populations and their drought tolerance (23) and biomass (fuel) continuity (24), thus also affecting fire regime responses to shorter term climate variability]. On interannual and shorter time scales, climate variability affects the flammability of live and dead forest vegetation (13–19, 25).

High-quality time series are essential for evaluating wildfire risks, but for various reasons (26), previous works have not rigorously documented changes in large-wildfire frequency for

<sup>1</sup> Scripps Institution of Oceanography, La Jolla, CA 92093, USA. <sup>2</sup> University of California, Merced, CA 95344, USA. <sup>3</sup> U.S. Geological Survey, La Jolla, CA 92093, USA. <sup>4</sup> Laboratory of Tree-Ring Research, University of Arizona, Tucson, AZ 85721, USA.

\*To whom correspondence should be addressed. E-mail: awesterling@ucmerced.edu